ADVANCED FUNCTIONAL MATERIALS
www.afm-journal.de

Check for updates

Water-Soluble Triazolium Ionic-Liquid-Induced Surface Self-Assembly to Enhance the Stability and Efficiency of Perovskite Solar Cells

Shuangjie Wang, Zhen Li, Yuanyuan Zhang, Xingrui Liu, Jian Han, Xuanhua Li, Zhike Liu, Shengzhong (Frank) Liu, and Wallace C. H. Choy*

Despite being a promising candidate for next-generation photovoltaics, perovskite solar cells (PSCs) exhibit limited stability that hinders their practical application. In order to improve the humidity stability of PSCs, herein, a series of ionic liquids (ILs) "1-alkyl-4-amino-1,2,4-triazolium" (termed as RATZ; R represents alkyl chain, and ATZ represents 4-amino-1,2,4-triazolium) as cations are designed and used as additives in methylammonium lead iodide ($MAPbI_3$) perovskite precursor solution, obtaining triazolium ILs-modified PSCs for the first time (termed as MA/RATZ PSCs). As opposed to from traditional methods that seek to improve the stability of PSCs by functionalizing perovskite film with hydrophobic molecules, humidity-stable perovskite films are prepared by exploiting the self-assembled monolayer (SAM) formation of water-soluble triazolium ILs on a hydrophilic perovskite surface. The mechanism is validated by experimental and theoretical calculation. This strategy means that the MA/RATZ devices exhibit good humidity stability, maintaining around 80% initial efficiency for 3500 h under 40 ± 5% relative humidity. Meanwhile, the MA/RATZ PSCs exhibit enhanced thermal stability and photostability. Tuning the molecule structure of the ILs additives achieves a maximum power conversion efficiency (PCE) of 20.03%. This work demonstrates the potential of using triazolium ILs as additives and SAM and molecular design to achieve high performance PSCs.

1. Introduction

Organic–inorganic hybrid perovskite materials have large absorption coefficients, bandgap tunability, and long charge-carrier diffusion length,[1–6] which render them tremendously attractive for photovoltaic and optoelectronic applications.[7–15] Since stability remains a huge challenge to the commercialization of perovskite solar cells (PSCs), it is of great significance to improve the stability and efficiency of PSCs at the same time.[16] Various materials have been reported for this task, such as polymers, fullerene, metal halide salts, organic halide salts, inorganic acids, solvents, and nanoparticles, etc.[17–22] Among these materials, ionic liquids (ILs), known as green solvents, have aroused considerable attentions as chemical additives for fabricating efficient PSCs,[23–25] due to their high thermal and electrochemical stability, nonvolatility, and high ionic conductivity.[26–28] In recent years, various of ILs have been used in PSCs fabrication, such as 1-butyl-3-methylimidazolium tetrafluoroborate,[29] 1-hexyl-3-methylimidazolium chloride,[30,31] 1-methyl-3-(1*H*, 1*H*, 2*H*, 2*H*-nonafluorohexyl)-imidazolium iodide,[32] 1-ethyl-3-methylimidazolium hexafluorophosphate,[33] and 1-benzyl-3-methylimidazolium chloride.[34] The ILs are beneficial to PSCs in two aspects: (1) ILs are used as interface modifiers to improve charge transfer and reduce current density–voltage (*J*–*V*) hysteresis; (2) ILs are used as chemical additives in perovskite precursors to regulate the processes of crystal nucleation and growth to achieve better morphologies and quality of films. Although the power conversion efficiency (PCE) of PSCs has been improved by ILs functionalizations, understanding the correlation between ILs structure

Dr. S. J. Wang, Prof. Z. Li, Dr. Y. Y. Zhang, Dr. X. R. Liu, Dr. J. Han, Prof. X. H. Li
State Key Laboratory of Solidification Processing
Center for Nano Energy Materials
School of Materials Science and Engineering
Northwestern Polytechnical University
and Shaanxi Joint Lab of Graphene (NPU)
Xi'an 710072, China
E-mail: lixh32@nwpu.edu.cn

The ORCID identification number(s) for the author(s) of this article can be found under https://doi.org/10.1002/adfm.201900417.

DOI: 10.1002/adfm.201900417

Prof. X. H. Li
Northwestern Polytechnical University-Queen Mary University of London (NPU-QMUL) Joint Research Institute of Advanced Materials and Structures (JRI-AMAS)
Xi'an 710072, China

Prof. Z. K. Liu, Prof. S. (Frank) Liu
School of Materials Science and Engineering
Shaanxi Normal University
Xi'an 710119, P. R. China

Prof. W. C. H. Choy
Department of Electrical and Electronic Engineering
The University of Hong Kong
Pokfulam Road, Hong Kong 999077, China

© 2019 WILEY-VCH Verlag GmbH & Co. KGaA, Weinheim

and device performance and additionally rational design of the ILs molecular structure are still lacking. Meanwhile, the effect of ILs on device stability has not been well studied.

During operation, substantial halide ion migration in PSCs generates vacancies and interstitial defects and forms positive charge Pb^{2+} defects on the surface of perovskite films, which leads to undesirable charge recombination and performance deterioration.[35] Molecules with $-NH_2$ group have shown the ability to passivate the unsaturated Pb^{2+} defects and reduce surface recombination.[36–38] Despite the tremendous advances in device PCE improvement, the humidity stability is still a significant concern for developing practical PSCs.[39,40] Recently, surface functionalization of perovskite films with hydrophobic molecules have been proved effective in improving their tolerance against humidity. For example, poly(methyl methacrylate),[41] liquid crystalline polymer,[42] alkylalkoxysilane,[43] polystyrene,[44,45] and fluoroalkyl silane,[46] have been used to enhance the humidity stability of PSCs. However, there is still a lack of research on the application of hydrophilic materials to improve the moisture tolerance of PSCs.

Herein, we designed ILs molecule with an amino group ($-NH_2$) and an adjustable alkyl side-chain, containing a cation of "1-alkyl-4-amino-1,2,4-triazolium" (termed as RATZ; R = ethyl, butyl, octyl, and ATZ represents 4-amino-1,2,4-triazolium) (**Scheme 1**a). Then, we incorporated these triazolium ILs into methylammonium lead iodide ($MAPbI_3$) perovskite precursor solution to form an active layer (termed as MA/RATZ; Scheme 1b). It is the first time of using triazolium ILs in PSCs to our knowledge. And distinct with the previously studied ILs in PSCs (Table S1 in the Supporting Information), our ILs all contain an amino group ($-NH_2$) with a lone electron pair, which tends to bond with Pb^{2+} defects on perovskite surface and achieve surface passivation. Encouragingly, a hydrophobic perovskite surface was achieved using the water-soluble triazolium ILs via the formation of self-assembled monolayer (SAM), which achieves the vertical alignment of alkyl chains along the surface of perovskite films and results in PSCs with significantly improved humidity stability (Scheme 1c). Ultimately, the PCE of the unencapsulated devices maintained close to 80% of their original efficiency after being exposed to 40 ± 5% relative humidity (RH) at room temperature and dark conditions for 3500 h. The MA/RATZ PSCs also exhibit good thermal stability and photostability. Correlation between the alkyl chain length of the ILs and the performance and stability of the PSCs was also studied and discussed. Additionally, we found that the presence of ILs increased the crystal size of perovskite (Scheme 1d). The incorporation of triazolium ILs was found to passivate trap states, increase conductivity, and promote carrier transportation and extraction in the perovskite films, which resulted in a significant improvement of the PCE from 16.13% to 20.03%.

2. Results and Discussion

We synthesized a series of triazolium ILs with different side-chain length. As shown in Scheme 1a (Experimental Section for details), the triazolium ILs were functionalized with $-C_2H_5$ (i.e., 1-ethyl-4-amino-1, 2, 4-triazolium iodine, [EATZ]I), $-C_4H_9$ (i.e., 1-butyl-4-amino-1, 2, 4-triazolium iodine, [BATZ]I), and $-C_8H_{17}$ (i.e., 1-octyl-4-amino-1, 2, 4-triazolium iodine, [OATZ]I) groups respectively. These triazolium ILs were confirmed by the ^1H NMR spectra, as illustrated in the Experimental Section. The solubility of [EATZ]I, [BATZ]I, and [OATZ]I in water are 88.5 g/100 g, 83.9 g/100 g, and 71.8 g/100 g, indicating good solubility of the triazolium ILs in water (**Figure 1**a). To investigate the effect of the triazolium ILs on the hydrophilicity/hydrophobicity of perovskite films surface, we measured the corresponding water contact angles. As depicted in Figure 1b(b1–b4), the control $MAPbI_3$ perovskite film exhibits a contact angle of around 67.7°, whereas those of MA/RATZ perovskite films are dramatically larger. Specifically, the water contact angles of the MA/EATZ, MA/BATZ, and MA/OATZ perovskite films are 91.2°, 95.7°, and 102.9°, respectively. The obvious increment in the water contact angle indicates that the surface of the MA/RATZ perovskite films are more hydrophobic, which could repel moisture and slow down water infiltration into the perovskite film in a moist environment.

To further confirm the water-soluble triazolium ILs-induced moisture resistance, the $MAPbI_3$ and MA/RATZ perovskite films were placed into a sealed box with RH of 80 ± 5%. The film degradation was monitored every few hours. The photographs of the degraded films are presented in Figure 1c(c1–c4). In high humidity conditions, the MA/RATZ perovskite films, especially the MA/OATZ film, maintained their original color for a prolonged time, even after 8 h of moist exposure, whereas the degradation of $MAPbI_3$ perovskite film progressed much faster and showed a light yellow color. Figure 1d–g illustrates the corresponding UV–vis spectra of the degraded films as a function of stored time under high humidity conditions. At the beginning of the experiment, all the perovskite films exhibited strong absorptions in the visible range from 400 to 750 nm. After being stored for 2 h, the absorption of the $MAPbI_3$ perovskite film dropped dramatically, which was consistent with the film color change from dark black to brown shown in Figure 1c(c1). After 8 h, the absorption at 400–750 nm almost disappeared completely, suggesting very poor humidity stability of the $MAPbI_3$ perovskite film. In contrast, the MA/RATZ perovskite films had improved stability against moisture, as was revealed by the little change of absorption intensity in Figure 1e–g.

To investigate the mechanism of the water-soluble triazolium ILs-induced hydrophilic-to-hydrophobic conversion of the perovskite films at molecular level, the surface chemistry of $MAPbI_3$ and MA/RATZ perovskite films were characterized by X-ray photoelectron spectroscopy (XPS) (**Figure 2**). Examination of the corresponding XPS survey spectra of C 1s, N 1s, I 3d, and Pb 4f revealed that no new peak appeared upon formation of the MA/RATZ perovskite films (Figure S1, Supporting Information).[47] To identify the chemical environment of lead and iodine, high-resolution XPS spectra of Pb 4f and I 3d of the perovskite films with and without triazolium ILs were investigated (Figure 2a; Figure S2, Supporting Information). Normally, two main peaks are observed in the spectra of Pb 4f and I 3d, i.e., the Pb $4f_{7/2}$ and Pb $4f_{5/2}$ peaks and the I $3d_{3/2}$ and I $3d_{5/2}$ peaks, respectively.[48] We observed that the Pb 4f peak in the $MAPbI_3$ perovskite film exhibited two small shoulders at the lower binding energy side of the main peak,

© 2019 WILEY-VCH Verlag GmbH & Co. KGaA, Weinheim

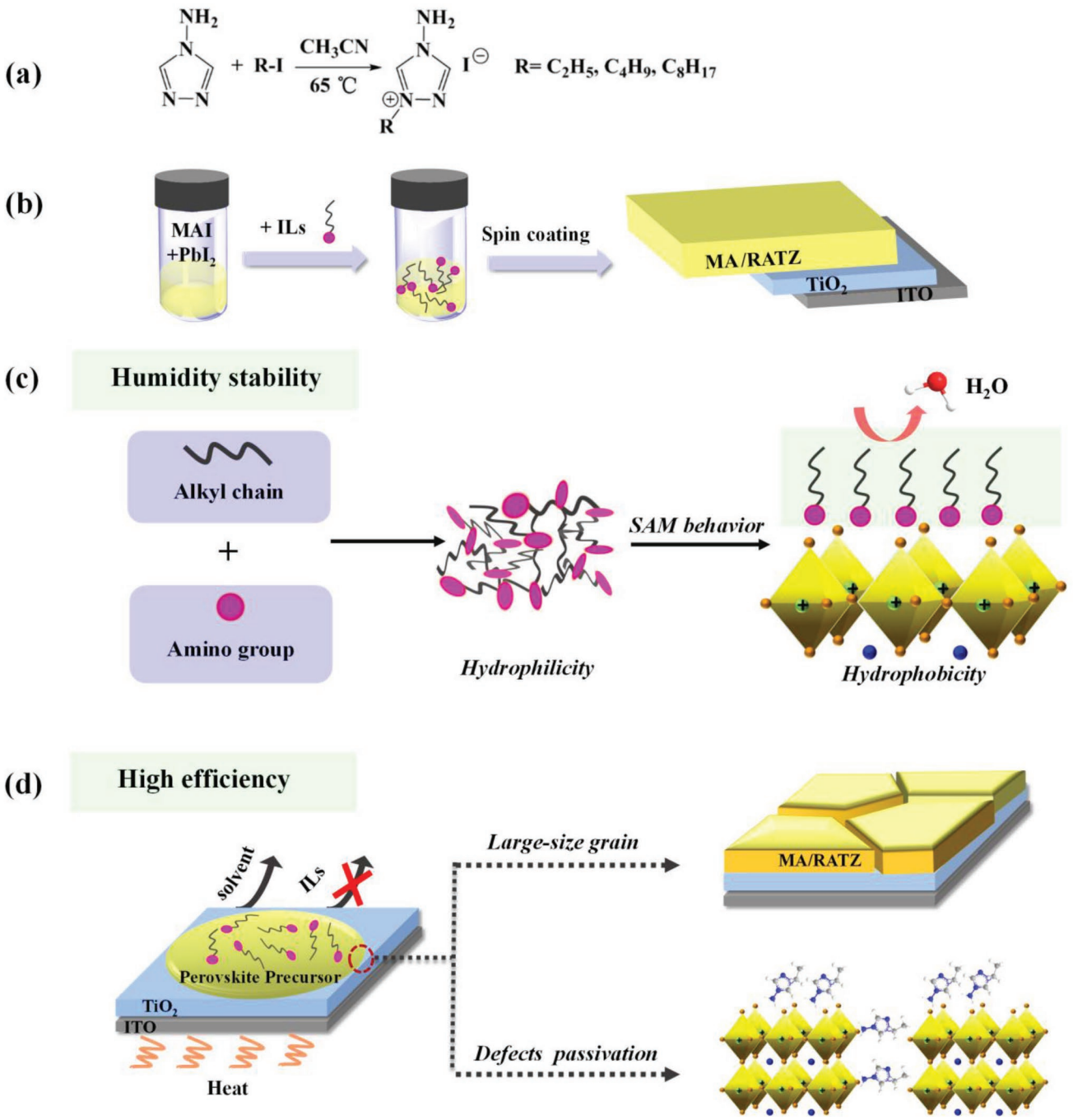

Scheme 1. a) The synthetic process of the three kinds of triazolium ILs with different alkyl chains. b) Schematic representation of preparation process of the MA/RATZ film as an active layer. Summary illustration of the role of triazolium ILs on the c) stability and d) efficiency improvement of PSCs.

marked with a red diamond in Figure 2a. According to the literatures, these small peaks could be attributed to metallic Pb due to the presence of unsaturated Pb^{2+} in $MAPbI_3$.[48–50] The unsaturated Pb^{2+} in the active layer could act as recombination centers and be detrimental to device performance.[51] In contrast, in the MA/RATZ perovskite films, the peaks assigned to unsaturated Pb^{2+} disappeared. Meanwhile, it is worth noting that the binding energy of Pb 4f has shifted 0.6, 0.5, and 0.3 eV to lower energy in the MA/EATZ, MA/BATZ, and MA/OATZ films, respectively. Whereas such shifts were not detected in I 3d XPS spectra (Figure S2, Supporting Information). These results could be explained by bond formation between Pb^{2+} and a functional group.

To further confirm the potential chemical bonding between triazolium ILs and Pb^{2+} in perovskite films, we performed theoretical calculations to investigate the interaction between ILs and perovskite film. Based on the molecular structure of the triazolium ILs and the spatial configuration of $MAPbI_3$, as illustrated

© 2019 WILEY-VCH Verlag GmbH & Co. KGaA, Weinheim

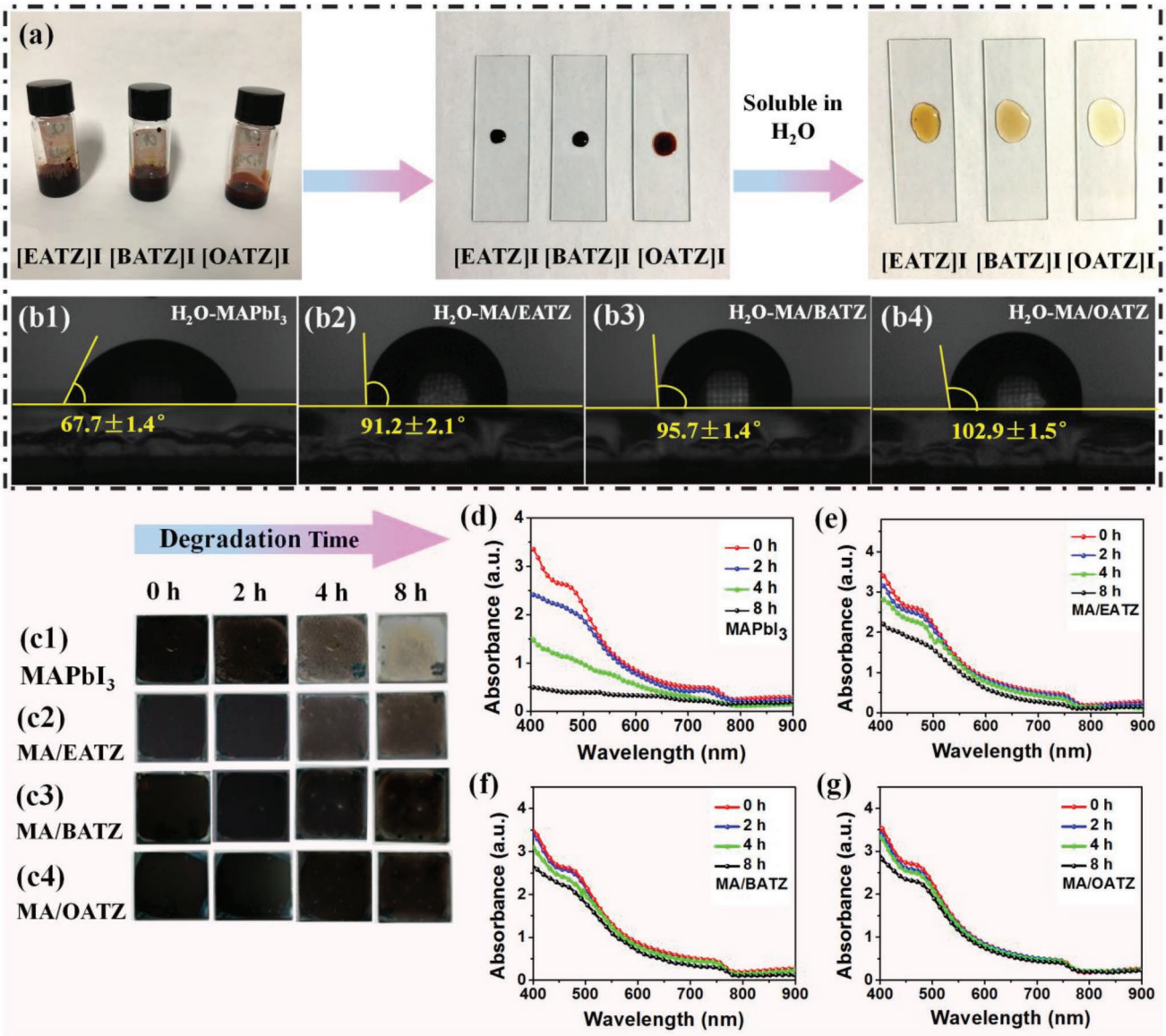

Figure 1. a) Schematic representation of water solubility of three kinds of triazolium ILs with different alkyl chains. Water contact angle measurements of the b1) $MAPbI_3$, b2) MA/EATZ, b3) MA/BATZ, and b4) MA/OATZ films. c) Photographs of the c1) $MAPbI_3$, c2) MA/EATZ, c3) MA/BATZ, and c4) MA/OATZ films after fully exposured to a RH of 80 ± 5% for 0, 2, 4, and 8 h at 25–30 °C. d–f) Monitoring perovskite degradation under RH of 80 ± 5% by UV–vis absorption spectroscopy of the d) $MAPbI_3$, e) MA/EATZ, f) MA/BATZ, and g) MA/OATZ films.

in Figure 2c–e and Figure S3 (Supporting Information), there could be three types of potential bonding configurations between the ILs and $MAPbI_3$: (1) the $-NH_2$ of ILs tends to bind to the Pb^{2+} at the perovskite film through the nitrogen lone electron pair; (2) the $-CH_2-$ linked to the N1 atom of 1,2,4-triazolium could bind to iodine in $MAPbI_3$ due to the electrostatic attraction; (3) the iodine could bind to $-CH_3$ at the end of the alkyl chain due to smaller space hindrance. Taking the case of MA/EATZ as an example (Figure 2c–e), we found that the total adsorption energy of the Pb–N bond is 1.16 eV lower than that of H–I bond (formed with $-CH_2-$) and 1.18 eV lower than that of another H–I bond (formed with $-CH_3$), indicating stronger and more stable binding between Pb and N. Consequently, the unsaturated Pb^{2+}, which is envisaged as responsible for the poor performance of PSCs, becomes more saturated through the Pb–N bond. In Figure S3 (Supporting Information), the type of bonding in MA/BATZ ($-CH_2-$: 1.46 eV, $-CH_3$: 1.23 eV) and MA/OATZ films ($-CH_2-$: 1.48 eV, $-CH_3$: 1.31 eV) is the same as that of MA/EATZ film. Based on the experimental results and theoretical calculation, it can be concluded that the amino group with a lone pair of electrons in the triazolium ILs forms Pb–N bonding with the unsaturated Pb^{2+} in the perovskite films (Figure 2b). The bonding further allows the ILs self-assemble as a monolayer on the perovskite surface with the alkyl chains vertically aligned along the perovskite surface (Scheme 1c). The SAM formation of the water-soluble triazolium ILs converted the hydrophilic perovskite films into hydrophobic ones.

© 2019 WILEY-VCH Verlag GmbH & Co. KGaA, Weinheim

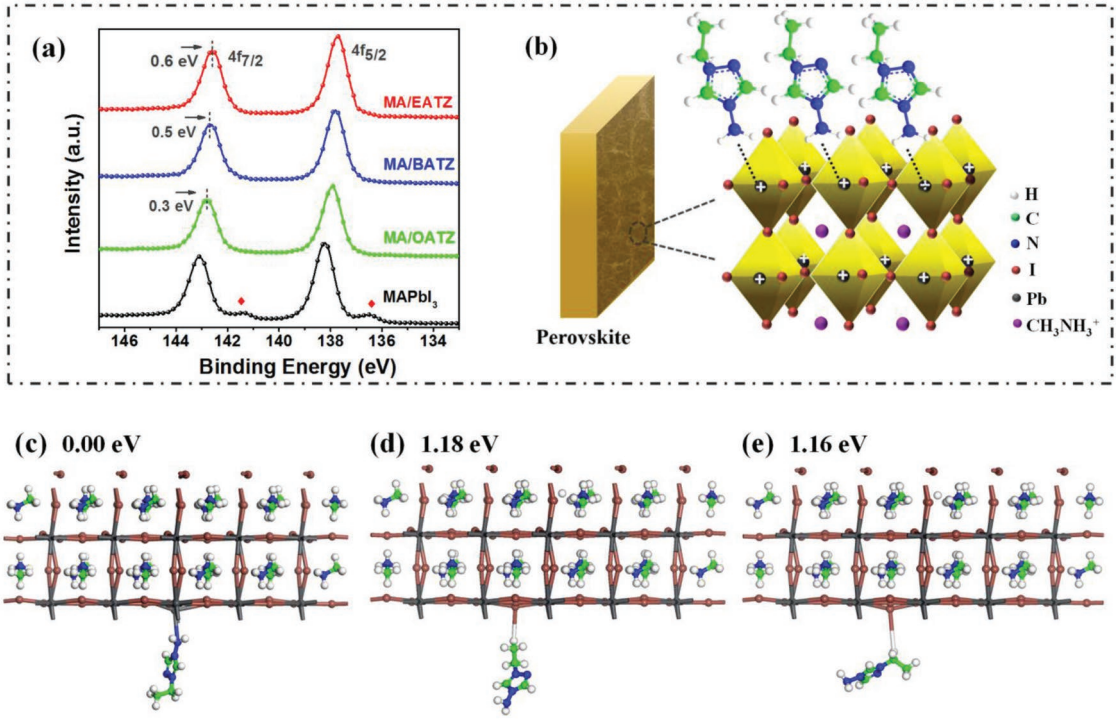

Figure 2. a) High-resolution XPS of Pb 4f core level measured on the $MAPbI_3$, MA/EATZ, MA/BATZ, and MA/OATZ films. b) Schematic of surface molecular structure of perovskite film and mechanism of SAM formation between $[EATZ]^+$ and perovskite film. c–e) Theoretical calculations: calculated adsorption of $[EATZ]^+$ within the triazolium ILs to the perovskite film. The relative energy of adsorption is provided.

Scanning electron microscopy (SEM) and atomic force microscopy (AFM) were deployed to study the microstructures of the devices. **Figure 3**a(a1–a4) shows the top-view SEM images of the $MAPbI_3$ and MA/RATZ perovskite films. All the perovskite films contain uniform grains with full coverage. Notably, enlarged grains are observed upon incorporation of triazolium ILs. The grain size distribution histograms along with the Gaussian fitting were evaluated and illustrated in Figure 3b(b1–b4). The average grain size of the $MAPbI_3$, MA/EATZ, MA/BATZ, and MA/OATZ perovskite films were determined to be ≈200, 400, 310, and 280 nm, respectively. Crystal structures of the perovskite films were studied with X-ray diffraction (XRD). As can be seen in **Figure 4**e, there is no observable peak shift or new peak appearance in the MA/RTZ perovskite films, which indicates that the large triazolium cations do not enter the $MAPbI_3$ lattice. The full width at half maximum (FWHM, inset of Figure 4e) of the XRD peak at about 14.1° decreased after introduction of the triazolium ILs, which is in accord with the grain size enlargement. The AFM results showed that the root-mean-square (RMS) roughness of the perovskite films did not change significantly upon modification with the triazolium ILs (Figure S4, Supporting Information), suggesting that the surface roughness does not contribute to the improvement of hydrophobicity of the films.

Two possible reasons are considered to explain the enhanced quality of the MA/RATZ perovskite films. On the one hand, as shown in Figure 3c(c1–c4), the contact angle of a droplet of $MAPbI_3$ perovskite precursor solution on the TiO_2 substrate is 27.5°, which decreases to 14.3°, 15.6°, and 17.3° after the incorporation of [EATZ]I, [BATZ]I, and [OATZ]I, respectively. The improved wettability implies lower surface energy at the solid/liquid interface, which is beneficial for improving the coverage of perovskite layer.[52] More importantly, the ILs are nonvolatile liquids due to their vapor pressure being close to zero. After evaporation of other solvents, a small amount of ILs remain in the perovskite films, which would slow down the crystal growth, resulting in larger grain size (Scheme 1d).[53]

The photovoltaic properties of the $MAPbI_3$ and MA/RATZ perovskite films were investigated using a device structure of indium tin oxides (ITO)/TiO_2/$MAPbI_3$ or (MA/RATZ)/spiro-OMeTAD/Au (note: spiro-OMeTAD represents 2,2′,7,7′-tetrakis(*N*, *N*-di-*p*-methoxyphenylamine)-9,9-spirobifluorene). The *J*–*V* characteristics were characterized under AM 1.5 G, 1 sun illumination. In addition, we systemically investigated the stability of devices with the variation of alkyl groups in the triazolium ILs. The relevant parameters are summarized in Figure 4 and **Table 1**, respectively. The control device, based on $MAPbI_3$ perovskite film, exhibited a short-circuit current (J_{sc}) of 21.82 mA cm^{-2}, an open-circuit voltage (V_{oc}) of 1.07 V, and a fill factor (FF) of 0.69 with a corresponding PCE of 16.13% (Figure 4a). The average performance parameters of ten devices are reported and all device PCEs were in the range of 13.00%–16.00% (the statistic distribution is provided in Figure S5 in the Supporting Information). For MA/RATZ PSCs, we first optimize the concentration of ILs additives based on device performance. The details of performance optimization with different triazolium ILs are shown in Tables S2–S4 and Figures S6–S8 in the Supporting Information. Among these devices, the optimized MA/EATZ device produced the highest V_{oc} of 1.10 V, J_{sc} of 23.39 mA cm^{-2}, and FF of 0.78, yielding

© 2019 WILEY-VCH Verlag GmbH & Co. KGaA, Weinheim

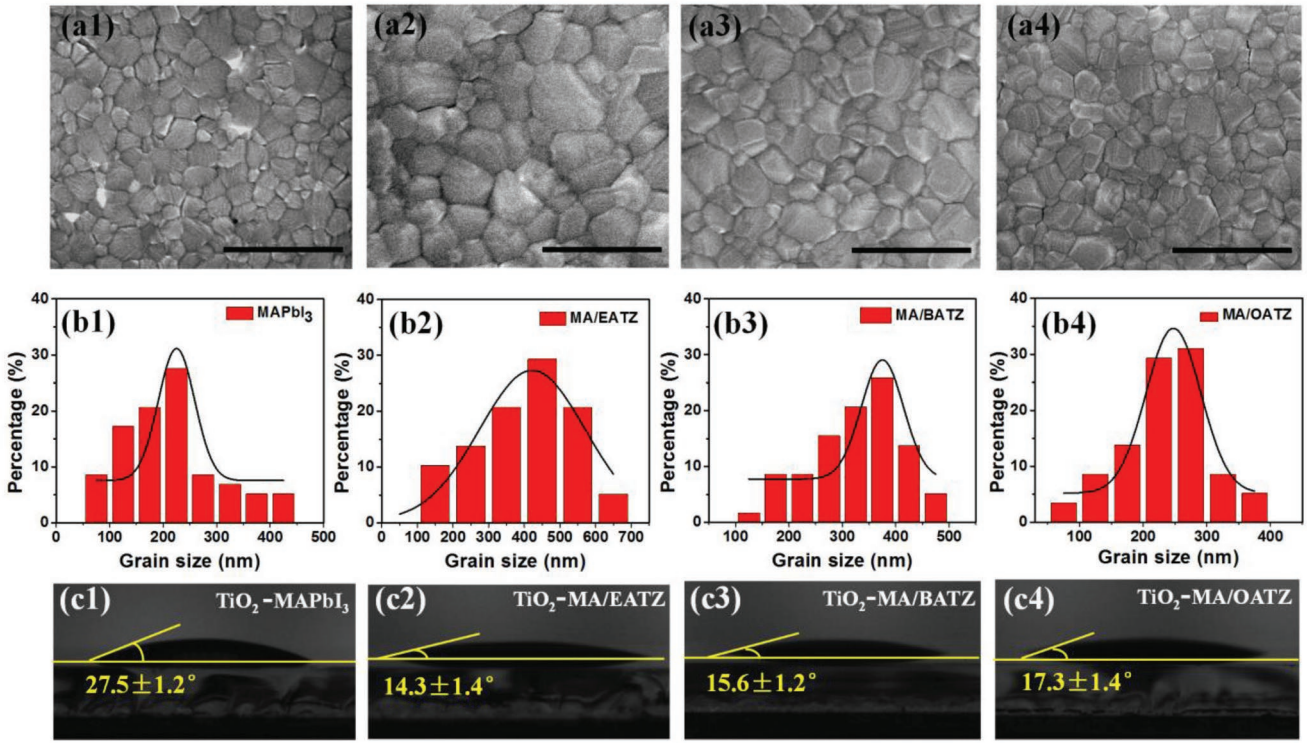

Figure 3. Top view SEM images and grain size distributions (obtained from SEM images) of the a1,b1) $MAPbI_3$, a2,b2) MA/EATZ, a3,b3) MA/BATZ, and a4,b4) MA/OATZ films. The scale bar in SEM images is 1 µm. c) Contact angel of c1) $MAPbI_3$, c2) MA/EATZ, c3) MA/BATZ, and c4) MA/OATZ precursor solution on TiO_2 film.

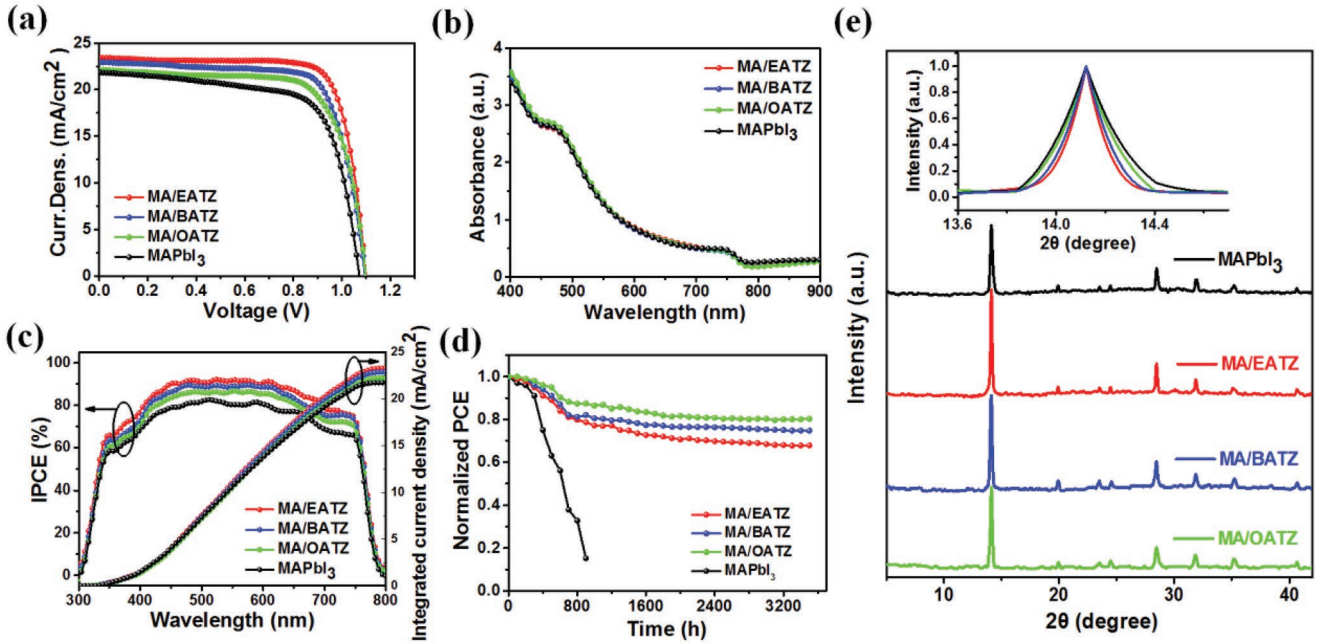

Figure 4. a) Current density–voltage (*J–V*) curves for the devices prepared from the different perovskite films measured under AM 1.5 G, 100 mW cm^{-2} illumination. b) UV–vis absorption spectra and c) IPCE spectra for the four types of PSCs. d) PCE of the four different devices normalized to the initial efficiencies as a function of storage time in dark and ambient atmosphere with 40 ± 5% relative humidity. e) XRD patterns for the four perovskite films. Inset: the enlarged drawing of the 13°–15° region of inset (e).

 © 2019 WILEY-VCH Verlag GmbH & Co. KGaA, Weinheim

Table 1. Statistical photovoltaic parameters of the $MAPbI_3$, MA/EATZ, MA/BATZ, and MA/OATZ devices.

	V_{oc} [V]	J_{sc} [mA cm^{-2}]	FF [%]	PCE [%]	R_s [Ω cm^{-2}]	R_{sh} [Ω cm^{-2}]
MA/EATZ	1.10 ± 0.01	23.39 ± 0.22	77.84 ± 0.14	20.03 ± 0.28	7.87 ± 0.84	2735.86 ± 39.00
MA/BATZ	1.10 ± 0.01	22.95 ± 0.32	74.83 ± 0.14	18.72 ± 0.60	8.75 ± 0.78	2264.97 ± 35.00
MA/OATZ	1.10 ± 0.01	22.18 ± 0.34	71.03 ± 0.13	17.33 ± 0.42	9.52 ± 0.70	1666.67 ± 41.00
$MAPbI_3$	1.07 ± 0.01	21.82 ± 0.45	69.00 ± 0.17	16.13 ± 0.41	10.07 ± 0.67	1085.19 ± 44.00

a PCE of 20.03%, which is among the best of the IL-modified PSCs (Table S1, Supporting Information). For the optimized MA/BATZ and MA/OATZ devices, the PSCs achieved PCEs of 18.72% and 17.33%, respectively. Regardless of the ILs types, the PCE of all modified PSCs with an optimized additive concentration was improved compared to the control $MAPbI_3$ PSC. The improvements can be mainly attributed to the increase of J_{sc} and FF. Figure S9 in the Supporting Information performs the steady-state measurements of J_{sc}, in which PCE outputs of over 15.95%, 19.43%, 17.88%, and 16.53% are obtained as a function of time at maximum power points of 0.86, 0.92, 0.88, and 0.87 V for $MAPbI_3$, MA/EATZ, MA/BATZ, and MA/OATZ devices, respectively. Additionally, the J–V hysteresis of the devices is reduced in the presence of triazolium ILs (Figure S10, Supporting Information), which is possible due to the decrease of trap-density in the active layers (discussed later) and better charge extraction at the TiO_2/perovskite interfaces.[31,54,55]

Next, the stability of the devices in humid environments was studied. The $MAPbI_3$ and optimized MA/RATZ PSCs were stored under a RH of around 40 ± 5% without encapsulation. As compared in Figure 4d, the PCE of $MAPbI_3$ device dropped precipitously after about 350 h of storage-stability test and performance loss was more than 70% after 800 h, whereas PCE of the MA/RATZ devices only decreased slightly. After 3500 h, the optimized MA/BATZ, and MA/OATZ devices remained close to 80% of their initial values. The high PCE retention of the MA/RATZ devices can be attributed to the hydrophobic surface of MA/RATZ perovskite films, which retards environmental water penetration into the active layer and thus prevents perovskite decomposition and device degradation. Likewise, the long-term stability of these unencapsulated devices under 80 ± 5% RH were also studied and the results are shown in Figure S11 in the Supporting Information. As expected, the MA/RATZ devices exhibited improved stability in contrast to the control $MAPbI_3$ device. The PCE of the $MAPbI_3$ device decayed drastically to 30% of initial value after about 50 h, while the devices with triazolium ILs retained over 80% of their original efficiency at the same test period. In particular, the retention of PCE in the case of the MA/OATZ in this high humidity ambient are still 80% after 300 h. Operational stability is another major concern for practical application of PSCs. The operational stability of our IL-modified PSCs were characterized by obtaining the PCE at maximum power point (MPP) voltage as a function of time under 1-sun illumination and at a RH of 40 ± 5%. As shown in Figure S12 in the Supporting Information, the $MAPbI_3$ device degraded more rapidly under operational conditions, losing 70% of their initial PCE over 17 h. However, the MA/RATZ devices exhibit higher durability than $MAPbI_3$ device, especially for the MA/EATZ device, retaining 80% of the initial PCE even after 30 h. It has been reported that formation of defects under illumination and ions migration under operational bias could be attributed to the accelerated degradation of PSCs under light.[56,57] The MA/EATZ device contains the best quality perovskite film with better crystallinity and reduced defect density (discussed later) among the investigated MA/RATZ devices, manifested from XRD and device performances. The better film quality reduces the possibility of defect formation and inhibits ion migration in the absorber layer under light illumination, therefore improves operational light stability. Additionally, we conducted a thermal stability test of $MAPbI_3$ and MA/RATZ devices without any encapsulation at 85 °C in nitrogen box (Figure S13, Supporting Information). With the addition of triazolium ILs, the PCEs of MA/RATZ devices show enhanced stability under continuous thermal stress. In particular, the MA/EATZ device retained ≈80% of original efficiency after about 35 h, while the $MAPbI_3$ device decreased to about 20% after about 30 h. Since grain boundaries in perovskite film are sensitive to thermal stress and act as high-speed channels for rapid diffusion of atomic, ionic, and molecular species, the perovskite degradation mainly propagates along the weakest grain boundaries of the films.[58] Thus, the MA/RATZ devices showed better thermal stability than $MAPbI_3$ device due to high quality perovskite films and defect passivation effect. Meanwhile, the unique thermal stability of ILs plays a positive role in devices at high temperatures.[27,59] Comparing the efficiencies and stabilities of the devices, it can be extracted that the MA/OATZ device exhibits lower efficiency but better humidity stability. The existence of the long alkyl chains in $[OATZ]^+$ could improve the moisture tolerance of perovskite film. On the other hand, the decreased PCE is mainly owing to the relatively low conductivity of the $[OATZ]^+$, leading to suboptimal electrical effects (see **Figure 5**). It is worth mentioning that the efficiency and stability results of our work are better than most of the state-of-the-art PSCs with ILs modifiers in recent year literatures (Table S1, Supporting Information).

Absorption spectra of the perovskite films with different ILs modifiers were investigated to rationalize the J_{sc} improvement in MA/RATZ devices. In Figure 4b, the absorption spectra of the MA/RATZ films are almost unchanged upon addition of ILs, indicating that the increased J_{sc} is not due to the light absorption enhancement. However, the incident photon-to-electron conversion efficiency (IPCE) spectra in Figure 4c show enhancement over the whole absorption region of 400–750 nm for the MA/RATZ films. Especially for the MA/EATZ film, a broad plateau over 90% is attained throughout the range of 400–750 nm. The calculated J_{sc} values from the IPCE were 21.73, 23.32, 22.91, and 22.16 mA cm^{-2} for the $MAPbI_3$, MA/EATZ, MA/BATZ, and MA/OATZ devices, respectively, which

© 2019 WILEY-VCH Verlag GmbH & Co. KGaA, Weinheim

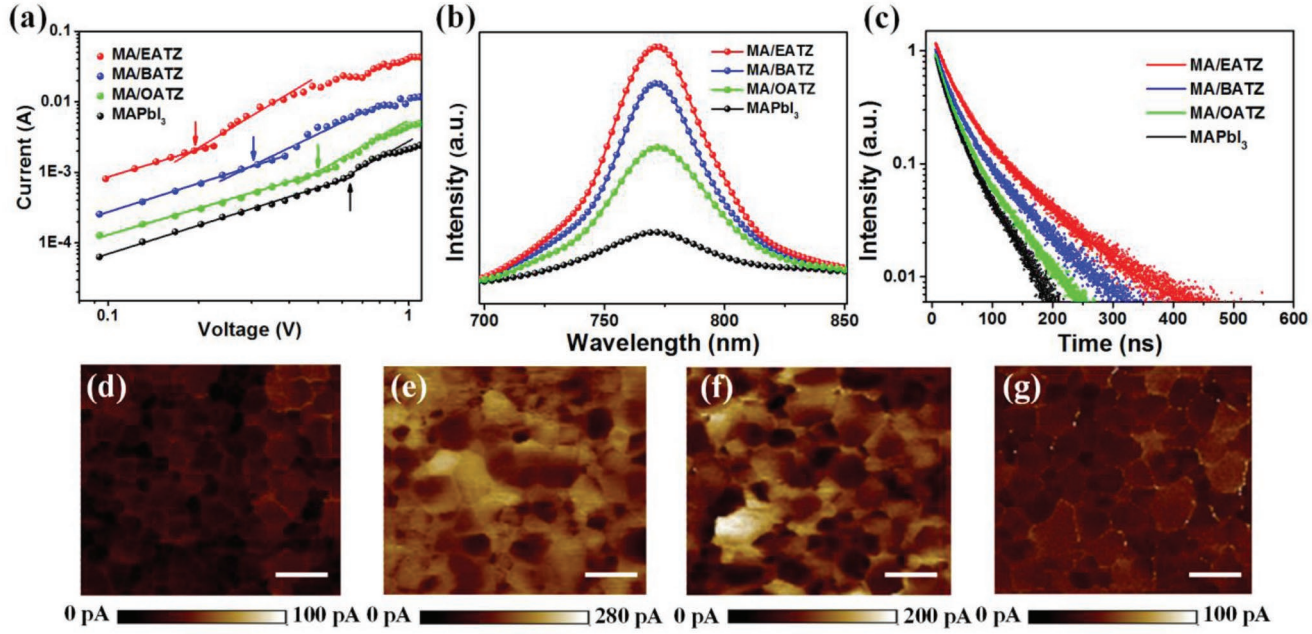

Figure 5. a) Dark *I–V* curves of the devices revealing V_{TFL} kink point, device structure: ITO/TiO_2/ $MAPbI_3$ or (MA/RATZ)/PCBM/Ag. b) Steady-state PL spectra and c) time-resolved PL decay curves of four different perovskite devices. The c-AFM topographic images of the d) $MAPbI_3$, e) MA/EATZ, f) MA/BATZ, and g) MA/OATZ active layer films recorded under dark and –0.3 V bias. The scale bar in c-AFM images is 500 nm. Note: under the same scale bar, the c-AFM topographic images of the four different active layer films recorded under dark and –0.3 V bias are shown in Figure S16 in the Supporting Information.

is in accord with the J_{sc} derived from the *J–V* measurements. Therefore, the substantial improvement in J_{sc} should be attributed to the positive electrical effects.

To understand the electronic property underlying the improved PCEs, we characterized the trap density in the active layer and obtained the log–log plots of the *I–V* curves. Figure 5a shows the *I–V* response of the films in ohmic-contacted configurations (ITO/TiO_2/ $MAPbI_3$ or (MA/RATZ)/PCBM/Ag) at low bias voltage range (note: PCBM represents [6,6]-phenyl-C61-butyric acid methyl ester). When the bias voltage exceeds the kink point, the current exhibits a nonlinear increase, indicating that the trap states are filled completely. Thus, the trap-filled limit voltage (V_{TFL}) is determined by the trap-state density (n_t) as follows[60]

$$V_{TFL} = \frac{en_t L^2}{2\varepsilon\varepsilon_0} \tag{1}$$

where e represents the elementary charge of the electron, L represents the thickness of the perovskite film, ε represents the relative dielectric constant of perovskite ($\varepsilon_{MAPbI3} = 28.8$),[61] and ε_0 represents the vacuum permittivity. From Figure 5a and Equation (1), the $MAPbI_3$ film exhibited a trap density of 3.22×10^{16} cm^{-3}, in good agreement with previous reports.[62] The trap density of the MA/EATZ, MA/BATZ, and MA/OATZ films were determined to be 1.03×10^{16} cm^{-3}, 1.64×10^{16} cm^{-3}, and 2.61×10^{16} cm^{-3}, respectively. The triazolium ILs incorporation can effectively passivate the traps in the active layers (Scheme 1d), resulting in enhanced device performance with improved J_{sc} and FF.

To characterize the charge-carrier kinetics, including carrier transportation and extraction, we measured the photoluminescence (PL) and time-resolved photoluminescence (TRPL) of the $MAPbI_3$ and MA/RATZ perovskite films. The PL and TRPL of $MAPbI_3$ (or MA/RATZ) absorber layers were measured and compared in Figure 5b,c. The PL position of all MA/RATZ perovskite films remained almost unchanged as compared to the $MAPbI_3$ perovskite films, with the peak position centered at around 770 nm. The MA/RATZ perovskite film exhibited stronger PL intensity compared to the control $MAPbI_3$ film, especially for the optimized MA/EATZ perovskite film. Figure 5c shows the TRPL spectra of the $MAPbI_3$ and MA/RATZ films. The MA/RATZ films exhibit longer PL lifetime compared to the $MAPbI_3$ reference. For the $MAPbI_3$ film, τ_{ave} was determined to be 30.87 ns. Upon triazolium ILs addition, τ_{ave} were increased to 64.04, 53.71, and 39.78 ns for the optimized MA/EATZ, MA/BATZ, and MA/OATZ films respectively, indicating less defects and charge recombination in the ILs-modified perovskites. These results further verify that triazolium ILs effectively reduces traps and inhibits charge recombination through the interaction between the amino group lone electron pair of the ILs and the unsaturated Pb^{2+} in perovskites. Accordingly, the *J–V* hysteresis of the MA/RATZ devices is effectively reduced (Figure S10, Supporting Information).

Electrochemical impedance spectroscopy (EIS) measurements have been performed to investigate the charge transfer processes of the devices. As shown in Figure S14 in the Supporting Information, the Nyquist plots of these devices based on $MAPbI_3$ and MA/RATZ perovskite films were conducted under dark condition with a forward bias of 0.8 V. It is known that the incomplete semicircle in the low frequency region is related to the recombination resistance (R_{rec}) and the semicircle in the high frequency region is correlated with the charge

 © 2019 WILEY-VCH Verlag GmbH & Co. KGaA, Weinheim

transfer resistance (R_{ct}).[63] According to the equivalent circuit, the fitting R_{rec} are 417, 1114, 801, and 573 Ω for $MAPbI_3$, MA/EATZ, MA/BATZ, and MA/OATZ, respectively. The R_{rec} for MA/RATZ devices are all higher than the $MAPbI_3$ device, especially for the MA/EATZ device. The higher R_{rec} of MA/RATZ cells indicates inhibition of recombination though triazolium ILs doping, which leads to increase of J_{sc} and FF in solar cells.

To gain further insights into the influence of the triazolium ILs on the electrical properties of the MA/RATZ films, conductive atomic force microscopy (c-AFM) was used to examine the conductivity of different active layers at nanometer scale.[64,65] The schematic diagram of c-AFM measurement for different perovskite films is shown in Figure S15 in the Supporting Information. The differences in local current distributions in the $MAPbI_3$ and MA/RATZ films are shown in Figure 5d–g. It is found that the local current in the films increased in the order of $MAPbI_3$, MA/OATZ, MA/BATZ, and MA/EATZ films. Two possible reasons can be attributed to the increased local current of the films, including the improved crystal quality of the MA/RATZ films and the high conductivity of these triazolium ILs. The conductivity of the [EATZ]I, [BATZ]I, and [OATZ] I were determined to be 2.07, 1.59, and 0.93 mS cm^{-1}. From the cationic point of view, the $[EATZ]^+$ cation with shorter ethyl chain has smaller spatial hindrance, which is conducive to the migration of cation and anion in ILs.[66] As a result, the conductivity of perovskite films was enhanced by the incorporation of triazolium ILs, especially the MA/EATZ films.

To sum up, the improved J_{sc} for the MA/RATZ devices could be attributed to efficient surface passivation, promoted carrier transportation and extraction, and increased conductivity of perovskite films. Meanwhile, the higher FF observed in the MA/RATZ devices stems most likely from the decreased series resistance (R_s) and increased shunt resistance (R_{sh}) shown in Figure S17 in the Supporting Information and Table 1.[29] The slight increase of V_{oc} from 1.07 to 1.10 V after the formation of the MA/RATZ films can be also attributed to reduced carrier recombination.

3. Conclusions

In conclusion, different triazolium ILs with amino have been synthesized and incorporated into perovskite precursor solution and successfully prepared MA/RATZ PSCs for the first time. We have also investigated the correlation between alkyl group length in the ILs and the performance and stability of PSCs. Despite being soluble in water, these ILs achieved hydrophobic perovskite films with enhanced humidity stability via formation of ILs SAM on the perovskite surface. Experimental and theoretical results indicate that mechanism for the hydrophobic conversion of perovskite film is related to the bonding of the amino ligands in the triazolium ILs to the unsaturated Pb^{2+} in the perovskite film, which prompted the SAM formation and vertical alignment of the hydrophobic alkyl chains along the surface of the perovskite film. In addition, the MA/RATZ PSCs exhibited improved thermal stability and photostability. Consequently, the MA/RATZ devices demonstrated enhanced stability and PCE compared to the $MAPbI_3$ device, especially in the case of MA/EATZ, which yielded a PCE up to 20.03%. The results demonstrated the great potentials of applying triazolium ILs in PSCs for improving both PCE and stability, which should be extendable to PSCs with other electron transport layers and active layers. With the flexible structural tunability of the ILs, triazolium ILs with different functionalities can be deployed in perovskite optoelectronic devices with improved performance and multiple functions in the future.

4. Experimental Section

Preparation of Triazolium ILs: In a 250 mL round-bottomed flask, 4-amino-1,2,4-triazolium and C_2H_5I having the molar ratio 1:3 were dissolved in the acetonitrile and the reaction was stirred at 323 K for 24 h. The flask was protected from light with a black bag. When 4-amino-1,2,4-triazolium had been consumed, the resultant solution was rotary evaporated until the volume did not change, viscous deep wine red solution was obtained. Then, the viscous solution was heated to 323 K for 12 h under vacuum. Eventually, [EATZ]I ILs was obtained in essentially quantitative yield and high purity obtained (>98.0%). Other triazolium ILs were synthesized according to the Scheme 1a by adopting the route of [EATZ]I. The ^1H NMR spectra of the triazolium ILs were recorded on a Bruker AVANCE 600 MHz (Germany), used $CDCl_3$ as locking solvent. Chemical shifts were reported in parts per million relative to TMS. ^1H NMR ([EATZ]I): 0.936 (t, 3H), 4.428 (t, 2H), 9.021 (s, 1H), 10.596 (s, 1H). ^1H NMR ([BATZ]I): 0.931 (t, 3H), 1.356-1.377 (m, 2H), 1.926 (m, 2H), 4.431 (t, 2H), 9.021 (s, 1H), 10.596 (s, 1H). ^1H NMR ([OATZ]I): 0.889 (t, 3H), 1.280-1.322 (m, 10H), 1.940 (m, 2H), 4.432 (t, 2H), 9.009 (s, 1H), 10.565 (s, 1H).

Device Fabrication: The MAI, PbI_2, and spiro-OMeTAD were purchased from Xi'an Polymer Light Technology Corp. and used as received without further purification. The C_2H_5I, C_4H_9I, $C_8H_{17}I$, and 4-amino-1,2,4-triazolium were purchased from Alfa Aesar. The device was fabricated with ITO/TiO_2/$MAPbI_3$ or (MA/RATZ)/spiro-OMeTAD/Au structures on patterned ITO glass through the following five steps. (1) Preparation of ITO electrode: ITO substrates (15 mm × 15 mm, 15 Ω sq^{-1} resistance) were cleaned with detergent and ultrasonicated in acetone and deionized water followed by ethanol. Then, the cleaned ITO substrates were dried with N_2 and treated in UV–ozone for 15 min to improve the ITO work function. (2) Preparation of electron transport layer (ETL): TiO_2 solution was chosen as an electron-transport material according to a previous method,[67] and coated on the cleaned ITO glasses by spin coating at 4000 rpm for 50 s, dried at 150 °C for 10 min. Then cooled down to room temperature. (3) Preparation of the $MAPbI_3$ or MA/RATZ perovskite films: the $MAPbI_3$ precursor solution was obtained by mixing MAI and PbI_2 (molar ratio = 1:1) in γ-butyrolactone and DMSO (7:3, v:v). For the MA/RATZ precursor solution, the different triazolium ILs were added with different molar percentage to MAI in $MAPbI_3$ precursor solution to obtain mixed solution. Sequentially, the $MAPbI_3$ or the MA/RATZ precursor solution was loaded on the ETL film at 3000 rpm for 50 s. Then, the substrate was drop-casted with chlorobenzene, heated at 100 °C for 10 min, and allowed to cool to room temperature. (4) Preparation of the hole transport layer (HTL): spiro-OMeTAD (75 mg) was dissolved in chlorobenzene (1 mL) containing 4-tBP (30 μL), and Li-TFSI (520 mg in 1 mL acetonitrile). The spiro-OMeTAD solution was deposited on top of the $MAPbI_3$ or MA/RATZ perovskite film at 4000 rpm for 40 s. The samples were kept in a desiccator overnight. (5) Preparation of the metal electrode: an 80 nm thick layer of gold was deposited on the HTL using thermal evaporator.

Characterization: The contact angles were measured using DSA100 (KRUSS, Germany). The sample morphology was characterized by SEM (FESEM, FEI, NANOSEM450, US) and AFM (Bruker Dimension Fastscan) using tapping mode with reflective probes resonating at a frequency of 150 kHz.[68–70] For c-AFM measurements, we chose ITO glass as substrate for spin coating $MAPbI_3$ or MA/RATZ film, and used Au-coated tips (13 kHz, 0.2 N m^{-1}) mounted on a 2 nA V^{-1} tip holder in contact mode under dark condition. XPS was performed on a Model K-Alpha

© 2019 WILEY-VCH Verlag GmbH & Co. KGaA, Weinheim

(Thermofisher Scientific Company, US) using a monochromated Al Kα source and a pass energy of 50 eV at a base pressure of 1×10^{-8} mbar. Absorption spectra of samples were obtained using a UV–vis–NIR spectrophotometer (Lambda 35, Perkin-Elmer). Photoluminescence (PL) of the membrane was carried out using a fluorescence spectrometer with 470 nm excitation (FLS 980), similar to previously report.[71,72] The TRPL spectra were acquired with a time-correlated single photon counting method using an Edinburgh Instruments FLS920 fluorescence spectrometer. The *J–V* characteristics of the device were measured employed a black metal mask under a solar simulator at AM 1.5 G illumination (100 mW cm^{-2}). The simulated light intensity was calibrated with a silicon photodiode. The IPCE spectra were measured with a monochromatic incident light in director current mode (1600 W, Newport). Electrochemical impedance spectroscopy measurement was performed on a model Solartron Analytical electrochemical analyzer (AMETEK, Inc. Berwyn, USA) in the frequency ranging from 1 MHz to 0.1 Hz, and the applied bias voltage was set as 0.8 V, respectively. The solubility of the different triazolium ILs in water was determined on the conductivity meter DDS-307 (DJS-1c platinum black electrode) and analytical balance (PT-104/55S) at $T = 298.15$ K. First, ultrapure water (100 g) was put into the flask equipped with conductivity meter. Then, a certain amount of triazolium ILs was added to the flask until the electrical conductivity remained constant. The above measurement was repeated three times, and the solubility was obtained by measuring the average mass of triazolium ILs. The conductivity of triazolium ILs was measured using conductivity meter DDS-307 at 298.15 K.

Details for Theoretical Calculations: The theoretical calculations were performed using the Material Studio with the Dmol3 module. The generalized gradient approximation (GGA) functional parameterized by Perdew–Burke–Ernzerhof (PBE).[73] The global orbital cutoff of 550 eV was considered in the calculations and the first Brillouin zone for the energy band calculation was performed using $2 \times 2 \times 1$ *k*-point meshes.[74] A $3 \times 3 \times 1$ supercell was adopted to investigate the adsorption of triazolium ILs. A smearing of 0.003 was used and the convergence of the total energy was set to be better than 10^{-5} Hartree. A vacuum layer with thickness of 20 Å was used to model the structure of perovskite.

Supporting Information

Supporting Information is available from the Wiley Online Library or from the author.

Acknowledgements

This research was supported by the Basic Research Fund for Free Exploration (JCYJ20170815161437298), the National Natural Science Foundation of China (51571166, 61505167, and 61701003), and the Key Scientific and Technological Team from Shaanxi Province (No. 2015KCT-12). The authors thank the support of the Project of Shaanxi Young Stars in Science and Technology (2017KJXX-18), and the Research Fund of the State Key Laboratory of Solidification Processing (NWPU) (Grant No. 147-QZ-2016).

Conflict of Interest

The authors declare no conflict of interest.

Keywords

perovskite solar cells, stability, surface self-assembly monolayer, triazolium ionic liquids

Received: January 14, 2019
Published online: February 18, 2019

[1] S. D. Stranks, G. E. Eperon, G. Grancini, C. Menelaou, M. J. P. Alcocer, T. Leijtens, L. M. Herz, A. Petrozza, H. J. Snaith, *Science* **2013**, *342*, 341.
[2] C. Wehrenfennig, G. E. Eperon, M. B. Johnston, H. J. Snaith, L. M. Herz, *Adv. Mater.* **2014**, *26*, 1584.
[3] Y. Fang, H. Wei, Q. Dong, J. Huang, *Nat. Commun.* **2017**, *8*, 14417.
[4] M. A. Green, A. Ho-Baillie, H. J. Snaith, *Nat. Photonics* **2014**, *8*, 506.
[5] Q. Lin, A. Armin, R. C. R. Nagiri, P. L. Burn, P. Meredith, *Nat. Photonics* **2015**, *9*, 106.
[6] M. Grätzel, *Nat. Mater.* **2014**, *13*, 838.
[7] M. Liu, M. B. Johnston, H. J. Snaith, *Nature* **2013**, *501*, 395.
[8] N. J. Jeon, J. H. Noh, Y. C. Kim, W. S. Yang, S. Ryu, S. I. Seok, *Nat. Mater.* **2014**, *13*, 897.
[9] M. Ahmadi, T. Wu, B. Hu, *Adv. Mater.* **2017**, *29*, 1605242.
[10] T. Singh, T. Miyasaka, *Adv. Energy Mater.* **2018**, *8*, 1700677.
[11] H. Zhou, Q. Chen, G. Li, S. Luo, T.-B. Song, H.-S. Duan, Z. Hong, J. You, Y. Liu, Y. Yang, *Science* **2014**, *345*, 542.
[12] N. J. Jeon, J. H. Noh, W. S. Yang, Y. C. Kim, S. Ryu, J. Seo, S. I. Seok, *Nature* **2015**, *517*, 476.
[13] D. Bi, C. Yi, J. Luo, J. D. Décoppet, F. Zhang, S. M. Zakeeruddin, X. Li, A. Hagfeldt, M. Grätzel, *Nat. Energy* **2016**, *1*, 16142.
[14] S. Wang, X. Li, T. Tong, J. Han, Y. Zhang, J. Zhu, Z. Huang, W. C. H. Choy, *Sol. RRL* **2018**, *2*, 1800027.
[15] M. M. Lee, J. Teuscher, T. Miyasaka, T. N. Murakami, H. J. Snaith, *Science* **2012**, *338*, 643.
[16] Z. Li, T. R. Klein, D. H. Kim, M. Yang, J. J. Berry, K. Zhu, *Nat. Rev. Mater.* **2018**, *3*, 18017.
[17] Y. Zhao, J. Wei, H. Li, Y. Yan, W. Zhou, D. Yu, Q. Zhao, *Nat. Commun.* **2016**, *7*, 10228.
[18] J. Xu, A. Buin, A. H. Ip, W. Li, O. Voznyy, R. Comin, M. Yuan, S. Jeon, Z. Ning, J. J. McDowell, P. Kanjanaboos, J. P. Sun, X. Lan, L. N. Quan, D. H. Kim, I. G. Hill, P. Maksymovych, E. H. Sargent, *Nat. Commun.* **2015**, *6*, 7081.
[19] M. Abdi-Jalebi, M. I. Dar, A. Sadhanala, S. P. Senanayak, M. Franckevičius, N. Arora, Y. Hu, S. M. Zakeeruddin, M. Grätzel, R. H. Friend, *Adv. Energy Mater.* **2016**, *6*, 1502472.
[20] Y. Guo, W. Sato, K. Shoyama, E. Nakamura, *J. Am. Chem. Soc.* **2016**, *138*, 5410.
[21] D. Bi, P. Gao, R. Scopelliti, E. Oveisi, J. Luo, M. Grätzel, A. Hagfeldt, M. K. Nazeeruddin, *Adv. Mater.* **2016**, *28*, 2910.
[22] W. Zhang, M. Saliba, S. D. Stranks, Y. Sun, X. Shi, U. Wiesner, H. J. Snaith, *Nano Lett.* **2013**, *13*, 4505.
[23] Y. Zhang, Z. Fei, P. Gao, Y. Lee, F. F. Tirani, R. Scopelliti, Y. Feng, P. J. Dyson, M. K. Nazeeruddin, *Adv. Mater.* **2017**, *29*, 1702157.
[24] Z. Fei, T. J. Geldbach, D. Zhao, P. J. Dyson, *Chem. - Eur. J.* **2006**, *12*, 2122.
[25] M. Salado, M. A. Fernandez, J. P. Holgado, S. Kazim, M. K. Nazeeruddin, P. J. Dyson, S. Ahmad, *ChemSusChem* **2017**, *10*, 3846.
[26] R. D. Rogers, K. R. Seddon, *Science* **2003**, *302*, 792.
[27] P. Hapiot, C. Lagrost, *Chem. Rev.* **2008**, *108*, 2238.
[28] M. Yoshizawa, W. Xu, C. A. Angell, *J. Am. Chem. Soc.* **2003**, *125*, 15411.
[29] D. Yang, X. Zhou, R. Yang, Z. Yang, W. Yu, X. Wang, C. Li, S. Liu, R. P. H. Chang, *Energy Environ. Sci.* **2016**, *9*, 3071.
[30] M. Shahiduzzaman, K. Yamamoto, Y. Furumoto, T. Kuwabara, K. Takahashi, T. Taima, *RSC Adv.* **2015**, *5*, 77495.
[31] M. Shahiduzzaman, K. Yamamoto, Y. Furumoto, T. Kuwabara, K. Takahashi, T. Taima, *Jpn. J. Appl. Phys.* **2016**, *55*, 02BF05.
[32] M. Salado, F. J. Ramos, V. M. Manzanares, P. Gao, M. K. Nazeeruddin, P. J. Dyson, S. Ahmad, *ChemSusChem* **2016**, *9*, 2708.
[33] Q. Wu, W. Zhou, Q. Liu, P. Zhou, T. Chen, Y. Lu, Q. Qiao, S. Yang, *ACS Appl. Mater. Interfaces* **2016**, *8*, 34464.
[34] D. Yang, R. Yang, X. Ren, X. Zhu, Z. Yang, C. Li, S. F. Liu, *Adv. Mater.* **2016**, *28*, 5206.

 © 2019 WILEY-VCH Verlag GmbH & Co. KGaA, Weinheim

[35] J. M. Azpiroz, E. Mosconi, J. Bisquert, F. De Angelis, *Energy Environ. Sci.* **2015**, *8*, 2118.
[36] Y. C. Shih, Y. B. Lan, C. S. Li, H. C. Hsieh, L. Wang, C. I. Wu, K. F. Lin, *Small* **2017**, *13*, 1604305.
[37] Y. Li, K. Lu, X. Ling, J. Yuan, G. Shi, G. Ding, J. Sun, S. Shi, X. Gong, W. Ma, *J. Mater. Chem. A* **2016**, *4*, 10130.
[38] C. Sun, Z. Wu, H.-L. Yip, H. Zhang, X.-F. Jiang, Q. Xue, Z. Hu, Z. Hu, Y. Shen, M. Wang, F. Huang, Y. Cao, *Adv. Energy Mater.* **2016**, *6*, 1501534.
[39] Y. Wang, T. Zhang, M. Kan, Y. Li, T. Wang, Y. Zhao, *Joule* **2018**, *2*, 2065.
[40] Y. Wang, T. Zhang, M. Kan, Y. Zhao, *J. Am. Chem. Soc.* **2018**, *140*, 12345.
[41] F. Wang, A. Shimazaki, F. Yang, K. Kanahashi, K. Matsuki, Y. Miyauchi, T. Takenobu, A. Wakamiya, Y. Murata, K. Matsuda, *J. Phys. Chem. C* **2017**, *121*, 1562.
[42] V. M. Arivunithi, S. S. Reddy, V. G. Sree, H.-Y. Park, J. Park, Y.-C. Kang, E.-S. Shin, Y.-Y. Noh, M. Song, S.-H. Jin, *Adv. Energy Mater.* **2018**, *8*, 1801637.
[43] J. Zhang, Z. Hu, L. Huang, G. Yue, J. Liu, X. Lu, Z. Hu, M. Shang, L. Han, Y. Zhu, *Chem. Commun.* **2015**, *51*, 7047.
[44] X. Wen, J. Wu, M. Ye, D. Gao, C. Lin, *Chem. Commun.* **2016**, *52*, 11355.
[45] P.-L. Qin, G. Yang, Z.-W. Ren, S. H. Cheung, S. K. So, L. Chen, J. Hao, J. Hou, G. Li, *Adv. Mater.* **2018**, *30*, 1706126.
[46] H. Xiong, Y. Rui, Y. Li, Q. Zhang, H. Wang, *J. Phys. Chem. C* **2016**, *4*, 6848.
[47] F. Giordano, A. Abate, J. P. Correa Baena, M. Saliba, T. Matsui, S. H. Im, S. M. Zakeeruddin, M. K. Nazeeruddin, A. Hagfeldt, M. Grätzel, *Nat. Commun.* **2016**, *7*, 10379.
[48] W. Zhang, S. Pathak, N. Sakai, T. Stergiopoulos, P. K. Nayak, N. K. Noel, A. A. Haghighirad, V. M. Burlakov, D. W. deQuilettes, A. Sadhanala, W. Li, L. Wang, D. S. Ginger, R. H. Friend, H. J. Snaith, *Nat. Commun.* **2015**, *6*, 10030.
[49] R. Lindblad, D. Bi, B. W. Park, J. Oscarsson, M. Gorgoi, H. Siegbahn, M. Odelius, E. M. Johansson, H. Rensmo, *J. Phys. Chem. Lett.* **2014**, *5*, 648.
[50] B. Conings, L. Baeten, J. D'Haen, J. Manca, H. G. Boyen, *Adv. Mater.* **2014**, *26*, 2041.
[51] G. Sadoughi, D. E. Starr, E. Handick, S. D. Stranks, M. Gorgoi, R. G. Wilks, M. Bar, H. J. Snaith, *ACS Appl. Mater. Interfaces* **2015**, *7*, 13440.
[52] T. Salim, S. Sun, Y. Abe, A. Krishna, A. C. Grimsdale, Y. M. Lam, *J. Mater. Chem. A* **2015**, *3*, 8943.
[53] J.-Y. Seo, T. Matsui, J. Luo, J.-P. Correa-Baena, F. Giordano, M. Saliba, K. Schenk, A. Ummadisingu, K. Domanski, M. Hadadian, A. Hagfeldt, S. M. Zakeeruddin, U. Steiner, M. Grätzel, A. Abate, *Adv. Energy Mater.* **2016**, *6*, 1600767.
[54] S. van Reenen, M. Kemerink, H. J. Snaith, *J. Phys. Chem. Lett.* **2015**, *6*, 3808.
[55] J. H. Heo, D. H. Song, H. J. Han, S. Y. Kim, J. H. Kim, D. Kim, H. W. Shin, T. K. Ahn, C. Wolf, T. W. Lee, S. H. Im, *Adv. Mater.* **2015**, *27*, 3424.
[56] J. W. Lee, Z. Dai, T. H. Han, C. Choi, S. Y. Chang, S. J. Lee, N. De Marco, H. Zhao, P. Sun, Y. Huang, Y. Yang, *Nat. Commun.* **2018**, *9*, 3021.
[57] K. Domanski, B. Roose, T. Matsui, M. Saliba, S.-H. Turren-Cruz, J.-P. Correa-Baena, C. R. Carmona, G. Richardson, J. M. Foster, F. De Angelis, J. M. Ball, A. Petrozza, N. Mine, M. K. Nazeeruddin, W. Tress, M. Grätzel, U. Steiner, A. Hagfeldt, A. Abate, *Energy Environ. Sci.* **2017**, *10*, 604.
[58] J. C. Yu, S. Badgujar, E. D. Jung, V. K. Singh, D. W. Kim, J. Gierschner, E. Lee, Y. S. Kim, S. Cho, M. S. Kwon, M. H. Song, *Adv. Mater.* **2018**, *30*, 1805554.
[59] M. Li, C. Zhao, Z.-K. Wang, C.-C. Zhang, H. K. H. Lee, A. Pockett, J. Barbé, W. C. Tsoi, Y.-G. Yang, M. J. Carnie, X.-Y. Gao, W.-X. Yang, J. R. Durrant, L.-S. Liao, S. M. Jain, *Adv. Energy Mater.* **2018**, *8*, 1801509.
[60] R. H. Bube, *J. Appl. Phys.* **1962**, *33*, 1733.
[61] A. Poglitsch, D. Weber, *J. Chem. Phys.* **1987**, *87*, 6373.
[62] Y. Shao, Z. Xiao, C. Bi, Y. Yuan, J. Huang, *Nat. Commun.* **2014**, *5*, 5784.
[63] H. Zheng, G. Liu, L. Zhu, J. Ye, X. Zhang, A. Alsaedi, T. Hayat, X. Pan, S. Dai, *ACS Appl. Mater. Interfaces* **2017**, *9*, 41006.
[64] G. Y. Kim, S. H. Oh, B. P. Nguyen, W. Jo, B. J. Kim, D. G. Lee, H. S. Jung, *J. Phys. Chem. Lett.* **2015**, *6*, 2355.
[65] J. Li, J. Ma, J. Hu, D. Wang, L. Wan, *ACS Appl. Mater. Interfaces* **2016**, *8*, 26002.
[66] Y. Wang, Y. Zhou, T. Zhang, M.-G. Ju, L. Zhang, M. Kan, Y. Li, X. Zeng, N. P. Padture, Y. Zhao, *Mater. Horiz.* **2018**, *5*, 868.
[67] X. Li, X. Ren, F. Xie, Y. Zhang, T. Xu, B. Wei, W. C. H. Choy, *Adv. Opt. Mater.* **2015**, *3*, 1220.
[68] X. Li, T. Tong, Q. Wu, S. Guo, Q. Song, J. Han, Z. Huang, *Adv. Funct. Mater.* **2018**, *28*, 1800475.
[69] S. Guo, X. Li, X. Ren, L. Yang, J. Zhu, B. Wei, *Adv. Funct. Mater.* **2018**, *28*, 1802567.
[70] J. Zhu, X. Li, Y. Zhang, J. Wang, B. Wei, *Adv. Funct. Mater.* **2018**, *28*, 1803872.
[71] T. Tong, X. Li, S. Guo, J. Han, B. Wei, *Nano Energy* **2017**, *41*, 591.
[72] X. Li, S. Guo, W. Li, X. Ren, J. Su, Q. Song, A. J. Sobrido, B. Wei, *Nano Energy* **2019**, *57*, 388.
[73] K. B. John, P. Perdew, M. Ernzerhof, *Phys. Rev. Lett.* **1996**, *77*, 3865.
[74] W. Setyawan, S. Curtarolo, *Comput. Mater. Sci.* **2010**, *49*, 299.

© 2019 WILEY-VCH Verlag GmbH & Co. KGaA, Weinheim